J Solid State Electrochem (2012) 16:2639–2649
DOI 10.1007/s10008-012-1688-5

ORIGINAL PAPER

Copolymer formation of 9-(2-(benzyloxy)ethyl)-9*H*-carbazole and 1-tosyl-1*H*-pyrrole coated on glassy carbon electrode and electrochemical impedance spectroscopy

Murat Ates · Nesimi Uludag · Tolga Karazehir

Received: 17 August 2011 / Revised: 11 February 2012 / Accepted: 13 February 2012 / Published online: 25 February 2012

Abstract In this work, 9-(2-(benzyloxy)ethyl)-9*H*-carbazole (BzOCz) and 1-tosyl-1*H*-pyrrole (TsP) monomers were chemically synthesized and characterized by Fourier transform infrared reflectance (FTIR) and proton nuclear magnetic resonance (^{1}H-NMR) spectroscopy. BzOCz and TsP were electrocoated on glassy carbon electrode (GCE) in various molar fractions (X_{TsP}=0.5, 0.83, 0.91, and 0.98) in 0.1 M sodium perchlorate/acetonitrile. The detailed characterization of poly (BzOCz-co-TsP) was studied by cyclic voltammetry, FTIR-attenuated total reflection spectroscopy and electrochemical impedance spectroscopy (EIS). The effects of different molar fractions during the preparation of modified electrodes were studied by EIS technique. The AC impedance technique was used to determine the capacitive behaviors of modified GCE via Nyquist, Bode magnitude, and Bode phase plots. The highest low frequency capacitance value was obtained as C_{LF}=23.94 μF cm^{-2} for X_{TsP}=0.98. Therefore, synthesized copolymer has more capacitive behavior than its homopolymers, such as C_{LF}=7.5 μF cm^{-2} for poly(BzOCz) and C_{LF}= 9.44 μF cm^{-2} for poly(TsP). In order to interpret the AC impedance spectra, R(Q(RW)) electrical equivalent circuit was employed with linear Kramers–Kronig test. A mechanism for electropolymerization has been proposed for copolymer formation.

M. Ates (✉) · N. Uludag · T. Karazehir
Department of Chemistry, Faculty of Arts and Sciences,
Namik Kemal University, Degirmenalti Campus,
59030 Tekirdag, Turkey
e-mail: mates@nku.edu.tr
URL: http://mates-en.nku.edu.tr/

T. Karazehir
Department of Chemistry, Istanbul Technical University,
Polymer Science and Technology,
Maslak,
34469 Istanbul, Turkey

Keywords Glassy carbon electrode · 9-(2-(benzyloxy) ethyl)-9*H*-carbazole · 1-tosyl-1*H*-pyrrole · Copolymerization · Electrochemical impedance spectroscopy · Circuit model

Introduction

Conducting polymers (CPs) are the subject of continuous research and development for potential applications [1], such as optical and electronic devices [2], organic transistors [3], electromagnetic shielding [4], energy storage systems [5], light emitting diodes [6], corrosion protection [7], sensors [8], and solar cells [9].

Electrochemical polymerization reactions have been studied for decades [10–12]. Although CPs can be polymerized by two methods via chemical and electrochemical techniques, they offer a better control over properties as they can be tailored by the changing experimental conditions, such as electrolyte, oxidation potential, solvent, etc. [13]. The electrochemical technique gives the opportunity of analytical investigations during the process of polymer formation and comparison of different polymers deposited on the same electrode under identical conditions.

Among conducting polymers, polycarbazole (PCz) has received considerable attention due to its high hole-transporting mobility of the charge carriers, and excellent electro-active and photo-active properties [14], environmental stability, photoconductivity, and electrical and electrochromic properties [15–22]. It is well-known that copolymerization is one of the most efficient approaches to modify the properties of CPs, which can produce copolymers with properties being intermediate between the individual polymers. By means of the electrochemical copolymerization, some new conducting polymers have

been prepared with several obvious advantages such as variation of electrical conductivity, enhancement of electrochemical activity, and improvement of thermal stability [23, 24]. The electrochemically polymerized PCz can exhibit interesting electrochromic properties in the presence of π-conjugated 3,6-linkages [25]. Wang et al. have carried out electrochemical copolymerization of carbazole (Cz) and dibenzo-18-crown-6 (DBC). They observed that copolymers possessed better thermal stability and higher electrical conductivity than those of poly(DBC) or PCz. Nie et al. performed copolymerization of Cz and 3-methylthiophene (3MeT). They showed that the insertion of 3MeT units into PCz was helpful in improving the conductivity of PCz and copolymers. Therefore, the copolymer has good redox activity, good thermal stability, and high conductivity. Sarac et al. have studied the copolymerization of methylpyrrole with ethylcarbazole [26] and methylcarbazole [27].

Thus, copolymerization could provide a convenient synthetic method and process for preparing new conducting materials with improved properties [28]. For the design of specific copolymeric systems and control of the degree of functionalization, it is important to be able to predict the copolymer composition, i.e., the relative proportions of each monomer constituent. This requires accurate knowledge of the relative reactivity of the two monomers toward a radical species and, in the case of electropolymerization, reactivity toward the electrode surface [29].

1-Tosyl-1*H*-pyrrole is a monomer bearing a sulfonyl group. Sulfonation of aromatic compounds is of great industrial importance due to the availability and low cost of the reagent. Consequently, sulfonation reactions have been studied extensively over the years, leading to the syntheses of a multitude of various aromatic sulfonyl derivatives [30, 31]. Recently, a novel one-pot synthesis of tosyl pyrrole derivatives, such as 1-tosyl-pyrrole, 1*H*-pyrrole-2(5H)-one, 5-hydroxy-1-tosyl-1*H*-pyrrole-2(5H)-one, and 5-oxo-1-tosyl-2,5-dihydro-1*H*-pyrrole-2-yl-acetate has been reported [32]. The synthesis and characterization of tosyl pyrrole have been already described in earlier papers [33–35], but the target molecule always was obtained in lower yields than in the present study. Papadopoulos et al. have synthesized 1-tosyl-1*H*-pyrrole (TsP) using metallic potassium salt in the yield of 84% [36]. In our study, due to the use of BuLi, a higher yield of TsP was obtained, which is of 94%. Copolymerization of different monomers either through chemical or electrochemical method can effectively modify the structures and properties of CPs [37]. One can obtain novel materials with controlled properties without suffering the experimental disadvantages associated to the synthesis of new homopolymers, e.g., complex synthetic routes to sophisticated monomers. Thus, it is an easy alternative to prepare copolymers with properties that are usually intermediate between those of individual homopolymers but significantly distinct from those of a composite or a blend.

In this study, the synthesis of 9-(2-(benzyloxy)ethyl)-9*H*-carbazole (BzOCz) and TsP monomers have been chemically synthesized. The monomers have been characterized by Fourier transform infrared reflectance (FTIR) and proton nuclear magnetic resonance (^{1}H-NMR) spectroscopy. Poly (BzOCz-co-TsP)/glassy carbon electrode (GCE) thin films have been obtained in different molar fractions (from X_{TsP}= 0.5 to X_{TsP}=0.98) by cyclic voltammetry (CV) method. Electrochemical impedance spectroscopy (EIS) analyses of modified electrode have been defined via Nyquist, Bode magnitude, and Bode phase plots.

Experimental

Materials

2-(9*H*-Carbazole-9-yl) ethanol (>95%), *p*-toluenesulfonyl chloride (>98%), pyrrole (>98%), triethylamine and sodium perchlorate (>98%), and butyl lithium (>97%) were obtained from Sigma-Aldrich. dichloromethane, silica gel (60 F254), acetonitrile, magnesium sulfate, hydrochloric acid, and tetrahydrofuran were purchased from Merck. All chemicals were high-grade reagents and were used as received.

Instrumentation

^{1}H-NMR spectra were recorded on a Varian Gemini 400 spectrometer, operating at 400 MHz. Spectra were registered in $CDCl_3$ using the solvent as internal standard at 400 MHz. Chemical shifts are expressed in terms of parts per million (δ) and the coupling constants are given in Hz. Infrared spectra were recorded by using Mattson 1000 FTIR spectrometer as KBr pellets. Melting points were determined in a capillary tube on Electro thermal IA 9000 apparatus. Reactions were monitored by thin layer chromatography

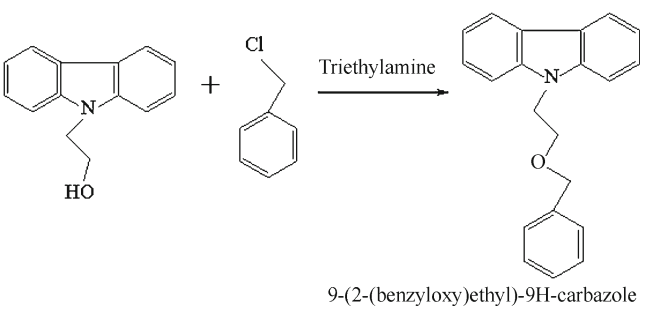

Fig. 1 Synthesis way of 9-(2-(benzyloxy)ethyl)-9*H*-carbazole monomer

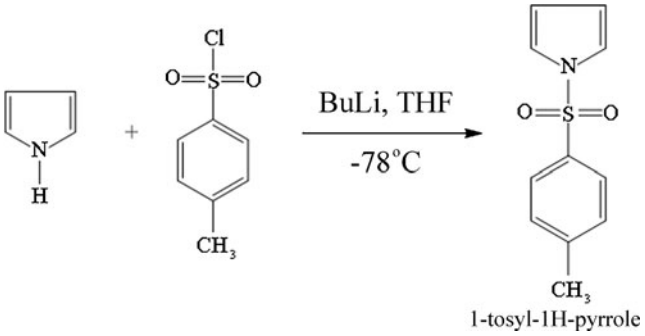

Fig. 2 Synthesis way of 1-tosyl-1*H*-pyrrole monomer

(silica gel 60 F254). Purification of solvents was performed according to standard methods.

Cyclic voltammetry was performed using a PARSTAT 2273 (software, power suit and Faraday cage, and BAS cell stand C_3) in a three-electrode electrochemical cell employing GCE (diameter=3 mm) as the working electrode, platinum disk electrode as the counter electrode, and Ag/AgCl (3.5 M) as the reference electrode.

Electrocoated polymer films were characterized by FTIR reflectance spectroscopy (Perkin Elmer, Spectrum One B, with an attenuated total reflection spectroscopy (ATR) attachment Universal ATR with ZnSe crystal). Modified carbon fiber microelectrodes (CFMEs) were washed in a solvent of acetonitrile.

Electro-synthesis procedure

Electropolymerization process was achieved by CV method at a scan rate of 100 mV s^{-1}. Electropolymerization experiments were done in 0.1 M sodium perchlorate ($NaClO_4$)/acetonitrile (ACN) containing different molar fraction ratios ($X_{TsP}=[TsP]_0/([TsP]_0+[BzOCz]_0)$ from $X_{TsP}=0.5$ to $X_{TsP}=0.98$ in the potential ranges from 0.00 to 1,800 mV at room temperature.

Electrochemical impedance spectroscopy

The EIS measurements were taken at room temperature (23± 2 °C) using a conventional three-electrode cell configuration. EIS measurements were conducted in monomer-free electrolyte solution with a perturbation amplitude 10 mV root mean square over a frequency range of 10 mHz to 100 kHz with PARSTAT 2273 (software; Powersuit).

Results and discussion

Synthesis of 9-(2-(benzyloxy)ethyl)-9*H*-carbazole

2-(9*H*-Carbazole-9-yl) ethanol (5.0 g, 23.7 mmol) was dissolved in 200 mL dichloromethane solution. The solution was cooled down to 0 °C. Triethylamine (1.7 mL, 12 mmol) was added to the solution. Benzyl chloride (5.5 mL, 47.37 mmol) was poured slowly and added over a period of 10 min. Afterwards, ice bath was removed and the mixture was allowed to stir at room temperature for 2 h. At the end of the chemical reaction period, unreacted benzyl chloride was extracted with 10% NaOH solution. After the extraction with 300 ml dichloromethane, the organic layer was dried over anhydrous Magnesium sulfate and evaporated, the residue was purified by Silica gel chromatography

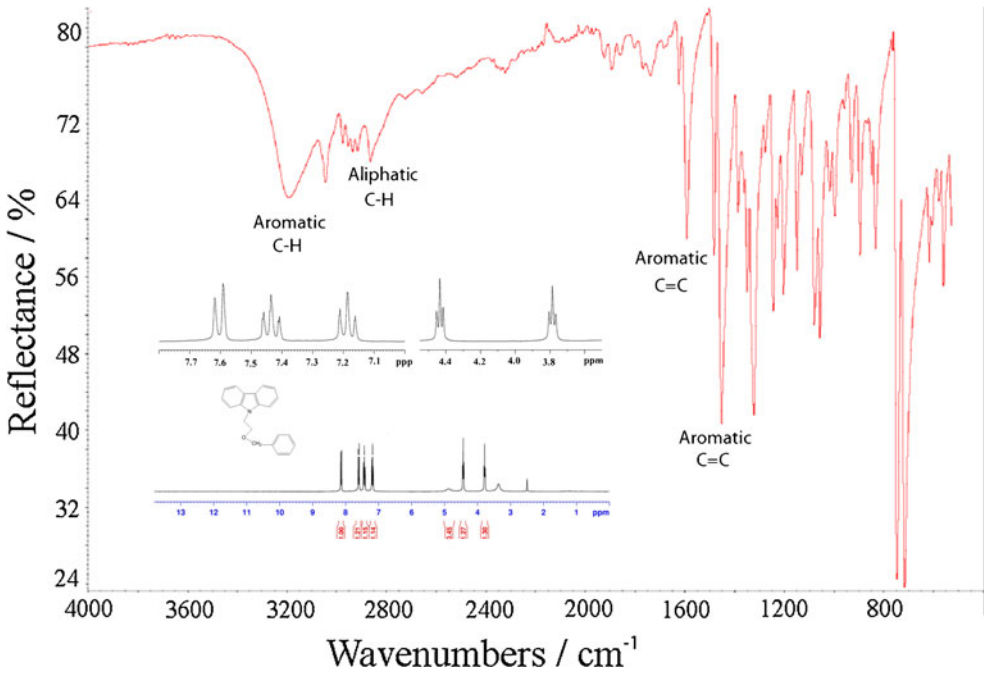

Fig. 3 FTIR spectrum of 9-(2-(benzyloxy)ethyl)-9*H*-carbazole monomer. *Inset* ^{1}H NMR ($CDCl_3$; 400 MHz) spectrum of 9-(2-(benzyloxy)ethyl)-9*H*-carbazole monomer

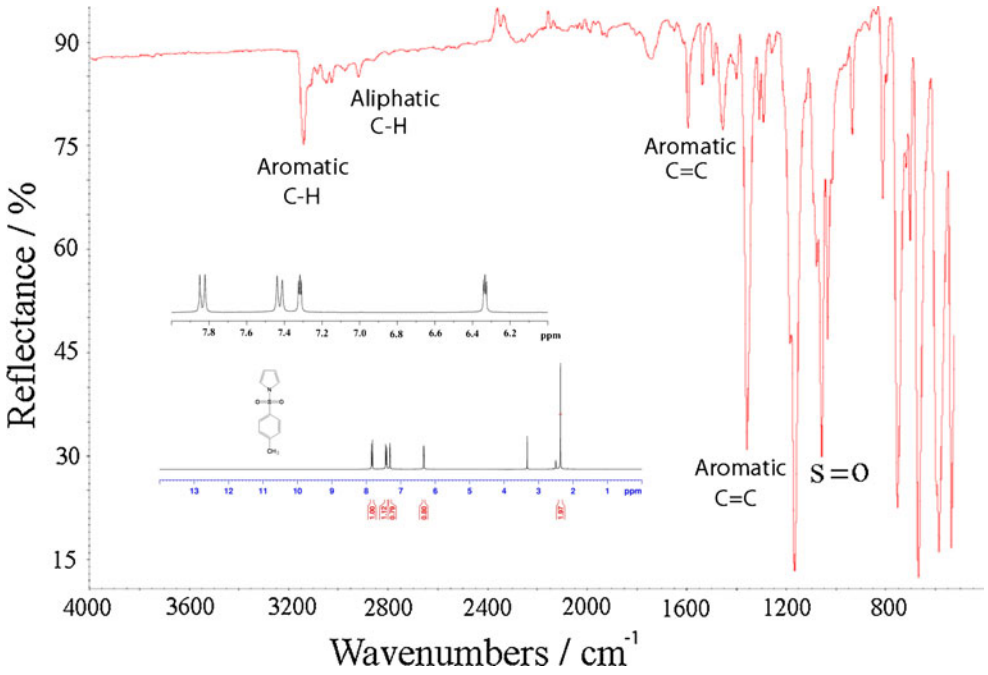

Fig. 4 FTIR spectrum of 1-tosyl-1*H*-pyrrole monomer. *Inset* ^{1}H NMR ($CDCl_3$; 400 MHz) spectrum of 1-tosyl-1*H*-pyrrole monomer

and crystallized from ethyl acetate (4.7 g) 65% of 9-(2-(benzyloxy)ethyl)-9*H*-carbazole (Fig. 1). Melting point was obtained as 83–85 °C.

Synthesis of 1-tosyl-1*H*-pyrrole

A solution of 3.48 ml (50 mmol) pyrrole in 200 ml tetrahydrofuran was cooled to −78 °C. After addition of 32.6 ml (52.3 mmol) *n*-butyl lithium, the resulting mixture was stirred for 30 min. After being stirred at −78 °C for 30 min, a solution of the *p*-toluenesulfonyl chloride 9.53 g (50 mmol) in 30 ml of anhydrous THF was added dropwise. The solution was allowed to warm overnight at room temperature for (~20 h). Then, the solution was poured into 300 ml of 10% water and brine solution, and then extracted with dichloromethane (100 ml). The organic layer was dried with anhydrous magnesium sulfate and the solvent was removed. The residue was purified by chromatography using silica gel and ethyl acetate. The product was recrystallized from ether to yield 10.25 g (94%) as a white solid; m.p. 108 °C, (Fig. 2).

Characterization of 9-(2-(benzyloxy)ethyl)-9*H*-carbazole monomer

In this study, 9-(2-(benzyloxy)ethyl)-9*H*-carbazole monomer was successfully synthesized in a higher yield of 65%. The FTIR spectrum (KBr) of 9-(2-(benzyloxy)ethyl)-9*H*-carbazole showed an absorption band due to the C–H aromatic (ν 3200 cm^{-1}), C–H aliphatic (2920 cm^{-1}), C=C aromatic (1580 and 1500 cm^{-1}; Fig. 3).

The most characteristic feature in ^{1}H-NMR ($CDCl_3$) spectra were dd at δ 8.3, 7.65–7.58 due to the aromatic proton, *m* at δ 7.5–7.4, 7.25–7.12 due to the aromatic proton and m δ 4.6–4.4 due to the CH_2, t δ 3.8 CH_2, s δ 2.5 CH_2 (inside of Fig. 3).

Analytical calculation for $C_{21}H_{19}NO$: C, 83,67; H, 6.35; N, 4.65.

Found: C, 83.64; H, 6.30; N, 4.68.

Characterization of 1-tosyl-1*H*-pyrrole monomer

The FTIR spectrum (KBr) of 1-tosyl-1*H*-pyrrole showed an absorption band due to the 3053 cm^{-1} (aromatic C-H) and

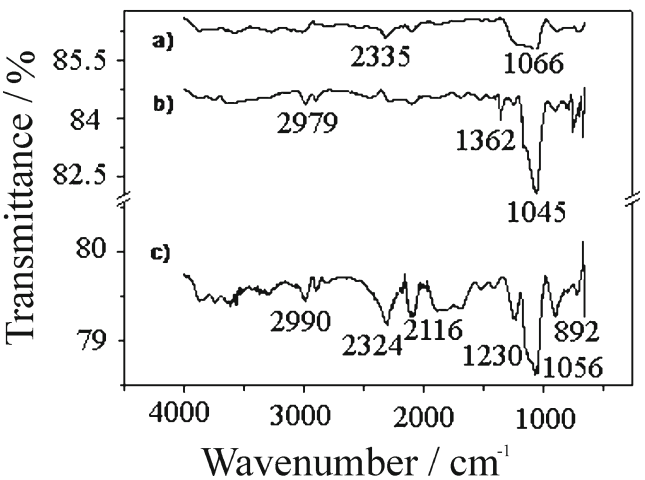

Fig. 5 FTIR–ATR spectrum of **a** poly(BzOCz)/GCE, $[BzOCz]_0$= 1 mM, **b** poly(TsP)/GCE, $[TsP]_0$=1 mM, **c** poly(BzOCz-co-TsP)/GCE, $[BzOCz]_0$=1 mM, and $[TsP]_0$=1 mM

2927 cm^{-1} (aliphatic C–H), 1500, 1420, 1380 cm^{-1} (aromatic C=C), 1168 cm^{-1} (S=O; Fig. 4). On the other hand, N–H band did not show absorption in 3400–3500 cm^{-1} region (pyrrole N–H stretching), the infrared spectrum has a strong band in the 1168 cm^{-1} (SO_2–N stretching) [36].

In the ^{1}H-NMR ($CDCl_3$) spectra of the 1-tosyl-1*H*-pyrrole, the methyl protons come from 3 ppm and aromatic protons due to the 7,8, 7,4, 7,3 and 6,5 ppm. On the other hand, N–H band did not show in 9–11 ppm (m, 4H, pyrrole proton C–H), 3.3 (s, 3H, CH_3) [38] (inside of Fig. 4). Finally, we have developed an efficient preparation of 1-tosyl-1H-pyrrole.

Analytical calculation for $C_{11}H_{11}NO_2S$: C, 59.70; H, 5.01; N, 6.34.

Found: C, 59.74; H, 5.00; N, 6.32.

FTIR–ATR analysis

The FTIR–ATR spectra of poly(BzOCz), poly(TsP), and poly(BzOCz-co-TsP) in molar fraction of X_{TsP}=0.5 were

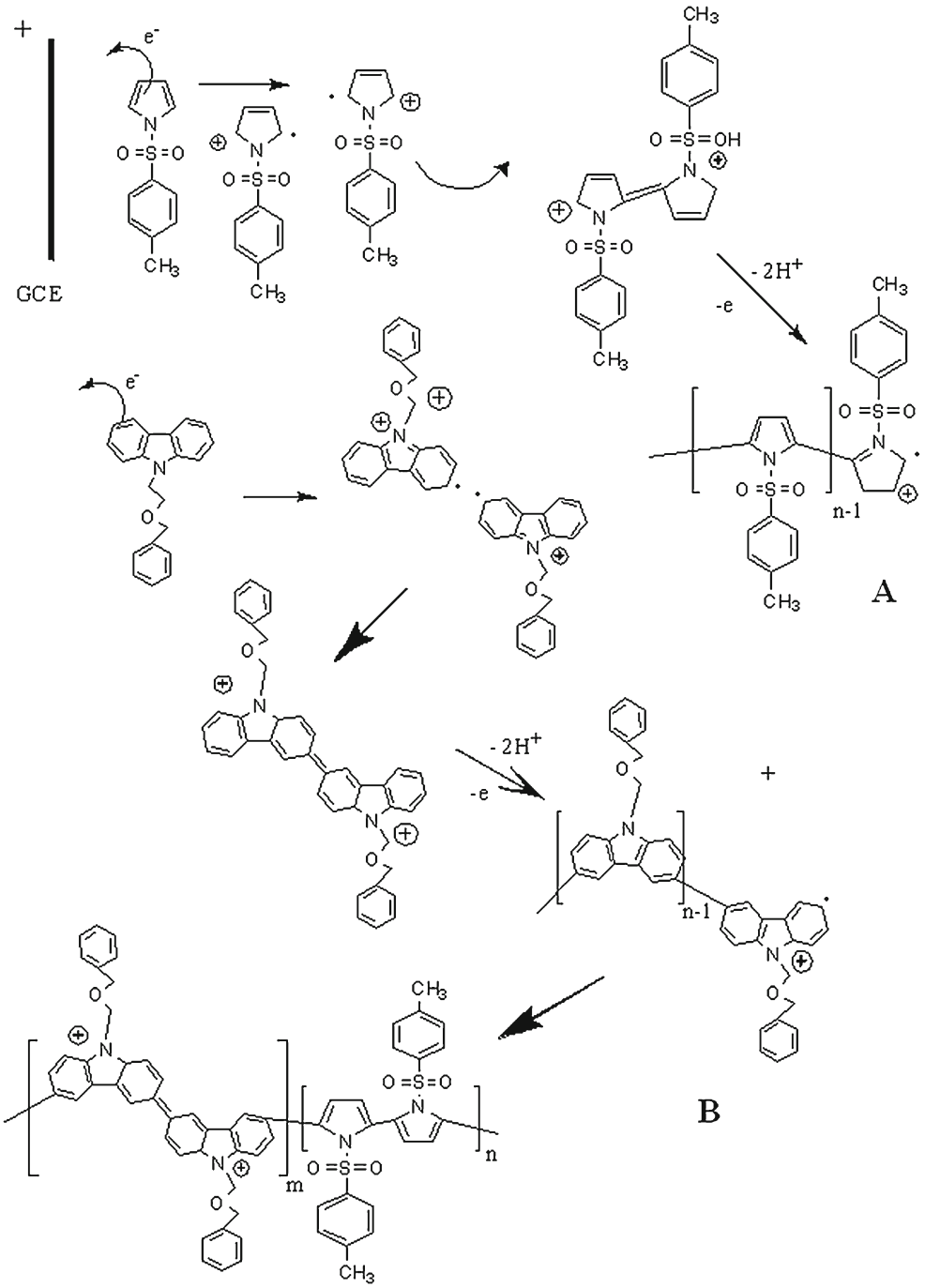

Fig. 6 Mechanism of Electrocopolymerization of BzOCz and TsP on GCE

obtained by reflectance FTIR measurements (Fig. 5). In the FTIR–ATR spectrum of poly(BzOCz-co-TsP), some shifts and some new peaks appearances are observed when it is compared to homopolymers. The band located at 1,362 cm^{-1} is confirmed by the valance vibration of C–N band of carbazole cycle [39]. The peaks 1066 cm^{-1} for poly(BzOCz), 1045 cm^{-1} for poly(TsP), and 1056 cm^{-1} for copolymer, which are attributed to dopant anion of ClO_4^- due to the doping of the electrolytes of $NaClO_4$/ACN [40]. The peaks at 2335 cm^{-1} for poly(BzOCz) and 2324 cm^{-1} for copolymer belong to aliphatic C–H. The peak at 892 cm^{-1} attributed to C–H deformation of out of plane of trisubstituted 1, 2, 4 carbazole cycle. The formation of copolymer was confirmed by FTIR–

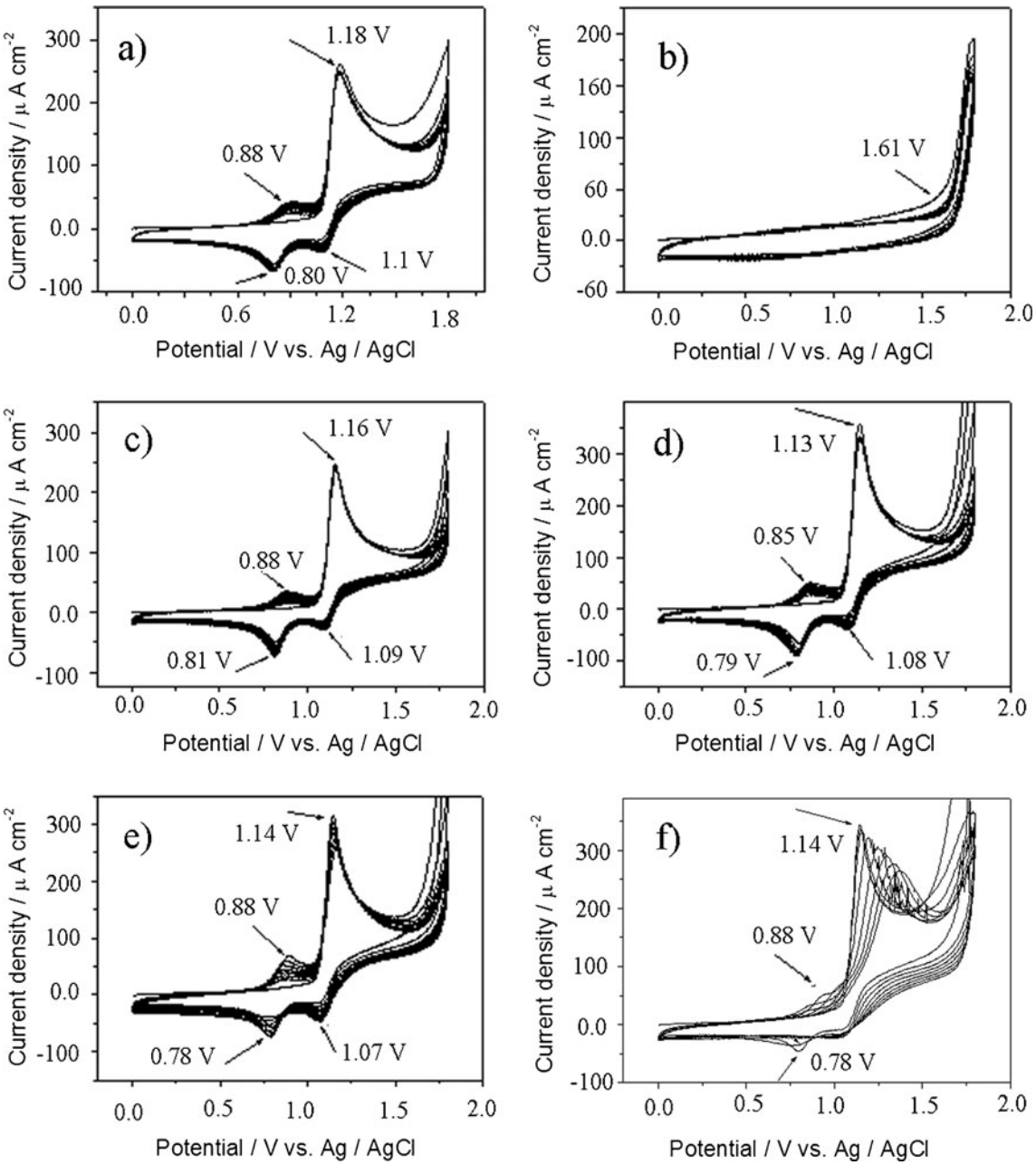

Fig. 7 Electrogrowth of **a** 9-(2-(benzyloxy)ethyl)-9*H*-carbazole (BzOCz), Q=4.325 mC, $[BzOCz]_0$=1 mM, **b** 1-tosyl-1*H*-pyrrole (TsP), Q=1.723 mC, $[TsP]_0$=1 mM, **c** poly(BzOCz-co-TsP), Q=3.571 mC, $[BzOCz]_0$=1 mM and $[TsP]_0$=1 mM, **d** poly(BzOCz-co-TsP), Q=5.437 mC, $[BzOCz]_0$=1 mM and $[TsP]_0$=5 mM, **e** poly (BzOCz-co-TsP), Q=5.065 mC, $[BzOCz]_0$=1 mM and $[TsP]_0$=10 mM, **f** poly(BzOCz-co-TsP), Q=6.516 mC, $[BzOCz]_0$=1 mM and $[TsP]_0$=50 mM. Scan rate: 100 mV s^{-1}, eight cycles, in 0.1 M $NaClO_4$/ACN

ATR images due to different peaks of homopolymers and copolymer.

Electropolymerization of homopolymers and copolymer

The electrochemical synthesis of co-polymer formation mechanism of BzOCz and TsP on GCE is shown in Fig. 6. The similar copolymer mechanism was given in our previous work [41]. The copolymerization occurs between 2 and/or 5 position of pyrrole and 3 and/or 6 position of carbazole derivative, cation formation by electron transfer from monomers to GCE. Radical cation coupling gives dimer formations of two monomers by electron and 2 mol H^+ elimination. Active radical cationic oligomers form. They added continuously in the electrogrowth process to form random copolymer. The mechanism of the electrocoated process depends on the experimental parameters especially on the solution type, electrode type, and the applied potential, etc [42].

Electrogrowth of 9-(2-(benzyloxy)ethyl)-9*H*-carbazole (Fig. 7a), 1-tosyl-1*H*-pyrrole (Fig. 7b), and copolymer of 9-(2-(benzyloxy)ethyl)-9*H*-carbazole and 1-tosyl-1*H*-pyrrole in the molar fraction ratio of X_{TsP}=0.5 (Fig. 7c), X_{TsP}=0.83 (Fig. 7d), X_{TsP}=0.91 (Fig. 7e), X_{TsP}=0.98 (Fig.7f) on GCE at a scan rate of 100 mV s^{-1}, eight cycles, in 0.1 M $NaClO_4$/ACN. The anodic and cathodic peak potentials are affected by the increasing of TsP monomer concentrations. Thus, we suggest that this reaction is a reversible system [43], especially for X_{TsP}=0.91 (Fig. 7e). The CV peaks also show that the values of monomer peak potential difference (ΔE_{mon}) and polymer peak potential difference (ΔE_{pol}) are below (ΔE=0.59 V/n) (Table 1). In the first CV cycle, the polymer oxidation peak at ~0.88 V and the monomer oxidation peak appear at ~1.18 V for BzOCz and only one oxidation peak at ~1.61 V for TsP. They are attributed to the radical cation formation using anodic potential of BzOCz and TsP monomers. Polymer oxidation peak potentials were nearly 0.88 V for X_{TsP}=0.5, X_{TsP}=0.91, and X_{TsP}=0.98. There is a little reduction amount of oxidation potential (0.85 V) for X_{TsP}=0.98. The CV of X_{TsP}=0.98 was distorted due to the higher amount of TsP. Monomer oxidation peak potentials for poly(BzOCz-co-TsP) at various molar fractions of TsP decreases to 1.16 V for X_{TsP}=0.5, 1.13 V for X_{TsP}=0.83, 1.14 V for X_{TsP}=0.91, and 1.14 V for X_{TsP}=0.98.

The peak separation between anodic and cathodic peak potentials (ΔE) during polymer growth was the highest for X_{TsP}=0.98 at a potential value of 0.36 V. It gives information about polymer thickness and the ion transport resistance involved in the redox reactions. The most coated thin film was obtained from electro-growth process (Q=6.516 mC). As a result, the most coated polymer film is thicker, so electron transfer between polymer and electrolyte will be slower.

Table 1 Redox parameters of electrogrowth of homopolymers and copolymers were obtained from CV

Mole fraction of X_{TsP}	ΔE_{mon}/V	ΔE_{pol}/V	Q/mC	$(\dot{I}_a/\dot{I}_c)_{mon}$	$(\dot{I}_a/\dot{I}_c)_{pol}$
Poly(BzOCz)	0.08	0.08	4.325	7.81	0.56
Poly(TsP)	–	–	1.723	–	–
Poly(BzOCz-co-TsP) X_{TsP}=0.5	0.07	0.07	3.571	8.0	0.42
X_{TsP}=0.83	0.05	0.06	5.437	8.81	0.58
X_{TsP}=0.91	0.07	0.10	5.065	5.85	0.91
X_{TsP}=0.98	–	0.36	6.516	–	6.61

Anodic and cathodic peak potential difference of polymers and monomers (ΔE/V), electrodeposition charge (Q/mC) and anodic and cathodic current density ratio (i_a/i_c) were determined

Effect of scan rate in monomer-free solution

Poly(BzOCz), poly(TsP), and poly(BzOCz-co-TsP)/GCE thin film was inserted into monomer-free electrolyte solution and its redox behavior was studied. One oxidation (~1.22 V) and one reduction peak (approximately −1.13 V) for poly(BzOCz), one oxidation (~1.19 V) and one reduction peak (approximately −0.90 V) for poly(TsP), and one oxidation (~1.22 V) and one reduction peak (approximately −0.79 V) for poly(BzOCz-co-TsP) were observed by increasing the applied potential by reverse scans in monomer-free electrolyte solution (Fig. 8a–f).

A reversible cyclic voltammogram is generally observed if both the oxidized and reduced species are stable and the kinetic of the electron transfer process is fast. The peak current (i_p) for a reversible voltammogram at 25 °C is given using the Randles–Sevčik equation: $i_p=(2.69\times10^5)\times A\times D^{1/2}\times C_0\times\nu^{1/2}$ where ν is the scan rate, A is electrode area, and D is the diffusion coefficient of electro-active species in the solution. The scan rate dependence of the anodic and cathodic peak currents shows a linear dependence on scan rate for poly (BzOCz), poly(TsP), and poly(BzOCz-co-TsP) against ν as shown in Fig. 8a, c, and e. This demonstrates that the electrochemical process has thin layer formation due to higher correlation coefficients R_{Anot}=0.95966, R_{Cat}=0.99086 (Fig. 8a), R_{Anot}=0.99589, R_{Cat}=0.99840 (Fig. 8c), R_{Anot}=0.97500, and R_{Cat}=0.97272 (Fig. 8e). Electrochemically modified polymer electrode shows linear dependency between scan rate and current density. It means that the polymer electrode process is a thin film formation. Peak current density is also proportional to $\nu^{1/2}$ in the range of scan rates, where it occurs by diffusion control [44] as given in Fig. 8b, d, and f. The correlation coefficient values were obtained as R_{Anot}=0.99306, R_{Cat}= 0.99395 (Fig. 8b), R_{Anot}=0.99658, R_{Cat}=0.99039 (Fig. 8d), R_{Anot}=0.99073, and R_{Cat}=0.99524 (Fig. 8f).

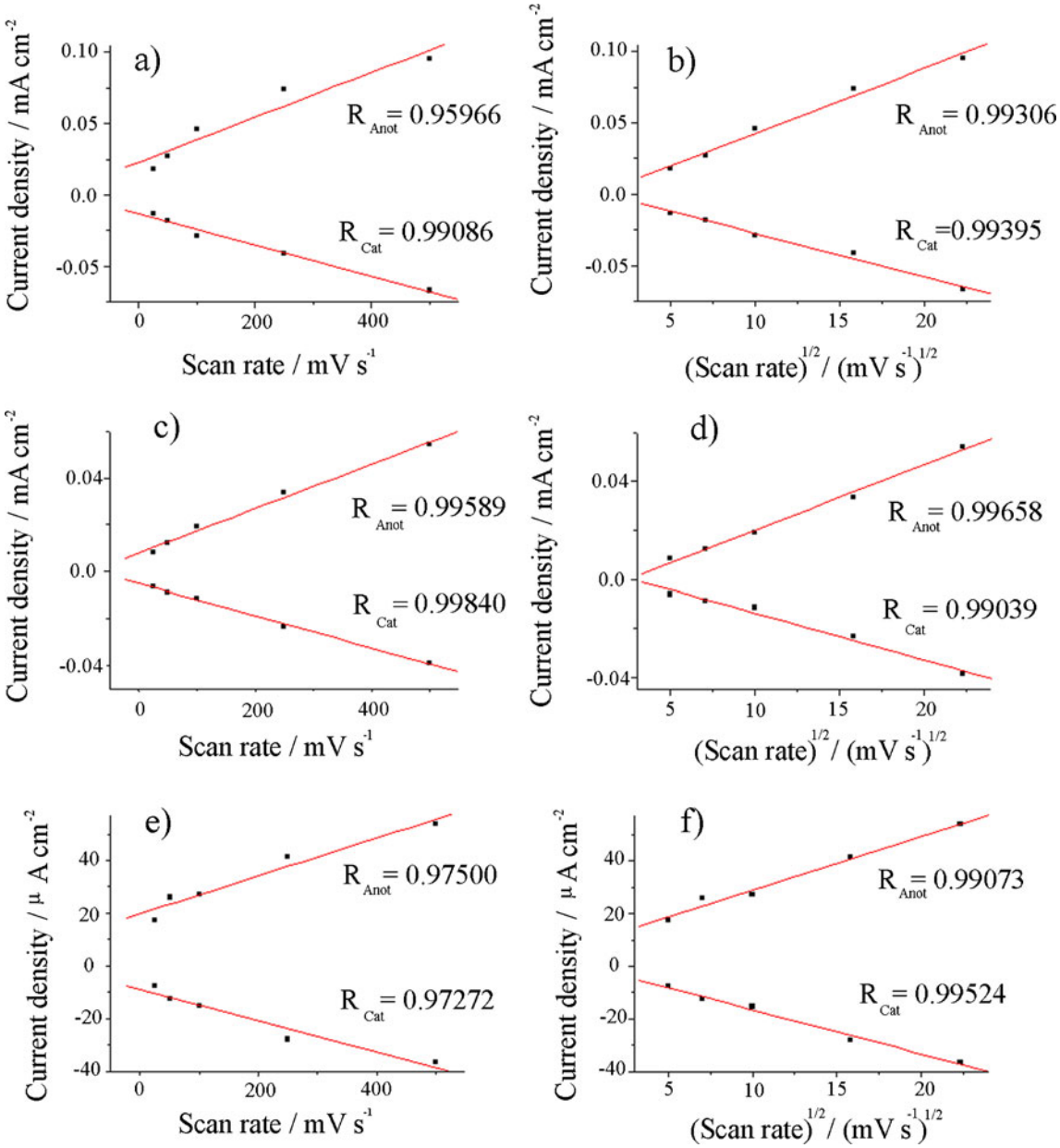

Fig. 8 **a** Scan rate dependence of poly(BzOCz), **b** plots of anodic and cathodic peak current density vs. the square root of scan rate dependence of poly(BzOCz), **c** scan rate dependence of poly(TsP), **d** Plots of anodic and cathodic peak current density vs. the square root of scan rate dependence of poly(TsP), **e** scan rate dependence of poly(BzOCz-co-TsP), **f** plots of anodic and cathodic peak current density vs. the square root of scan rate dependence of poly(BzOCz-co-TsP). All measurements are taken in monomer-free solution in 0.1 M $NaClO_4$/ACN. Scan rates were given from 25 to 500 mV s^{-1}

Electrochemical impedance spectroscopic study

The electrochemical impedance data is often given by use of Nyquist plot, shown in Fig. 9, which plots the Z' and Z'' of the impedance on x- and y-axis, respectively. Impedance measurements were carried out on the polymer/electrolyte systems at room temperature. All electrodes show a deviation from the capacitive line (Z''), indicating fast charge transfer at the GCE/(co)polymer and (co)polymer/solution interfaces, as well as fast charge transport in the polymer bulk. The increase in steepness in Nyquist plot is given in Fig. 9.

Nyquist plot for poly(BzOCz), poly(TsP) and poly (BzOCz-co-TsP) indicate the highest low frequency capacitive behavior at the frequency of 0.01 Hz in the molar fraction of X_{TsP}=0.98 as 23.94 μF cm^{-2}. The lowest frequency (f) value (0.01 Hz) and the highest Z_{im} (Z'') values put in the formula: $C_{LF}=1/2\times\pi\times f\times Z''_{im}$ to obtain for low

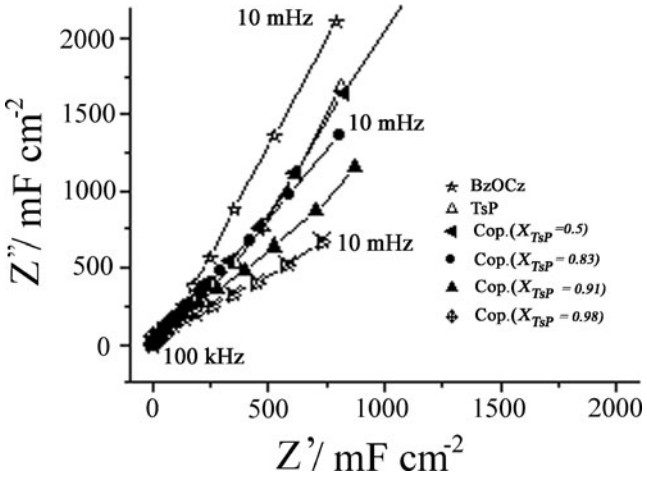

Fig. 9 Nyquist plots for poly(BzOCz), poly(TsP) and poly(BzOCz-co-TsP) as X_{TsP}=0.5, 0.83, 0.91, and 0.98, respectively

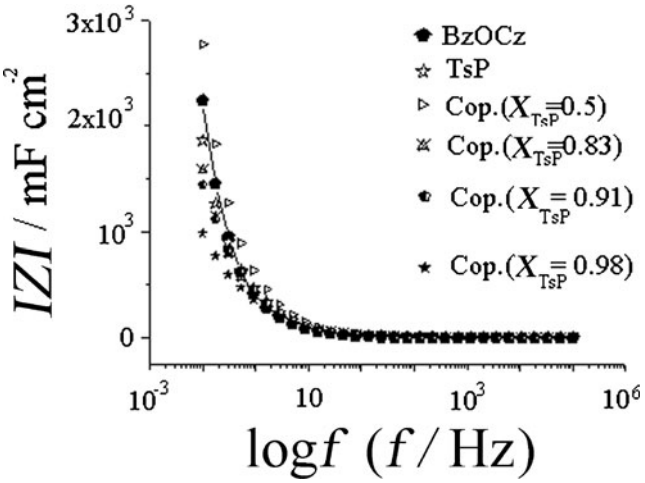

Fig. 10 Bode magnitude plot for poly(BzOCz), poly(TsP) and poly (BzOCz-co-TsP) as X_{TsP}=0.5, 0.83, 0.91, and 0.98, respectively

frequency capacitance results. The C_{LF} results can be obtained as 7.5, 9.44, 6.36, 11.65, 13.97 μF cm^{-2} for poly (BzOCz), poly(TsP), and poly(BzOCz-co-TsP) as X_{TsP}=0.5, 0.83, and 0.91, respectively. C_{LF} has been obtained in higher value than its homopolymers especially for X_{TsP}=0.98. In previous studies, poly(TsCz)/CFME indicates the highest C_{LF}=50 mF cm^{-2} in 0.1 M $NaClO_4$/ACN in the initial monomer concentration of 10 mM [44]. Poly(vinylbenzyl carbazole)/CFME shows a higher C_{LF}=564.1 μF cm^{-2} and C_{dl}=108 μF cm^{-2} in the initial monomer concentration of 10 mM in 0.1 M $LiClO_4$/ACN [43]. All impedance spectra show Warburg impedance at high frequencies, a transition to a capacitive behavior at medium frequencies and an approximately–capacitive line at low frequencies. In our EIS system, the minimum frequency was taken at 0.01 Hz [45].

A value of double layer capacitance, C_{dl}, can be calculated from a Bode magnitude plot by extrapolating the linear section to a value of ω=1 (log w=0) and employing the relationship IZI=1/C_{dl}, as shown in Fig. 10.

Double layer capacitance values (C_{dl}=~14.0 μF cm^{-2}) were nearly obtained for poly(BzOCz), poly(TsP), and poly (BzOCz-co-TsP) as X_{TsP}=0.5, 0.83, 0.91, and 0.98, respectively. C_{dl} value is higher than poly(9-tosyl-9*H*-carbazole) [44] (C_{dl}=11.0 μF cm^{-2}) in the initial monomer concentration of 10 mM. Higher C_{dl} values were obtained for poly(9-(4-vinylbenzyl)-9*H*-carbazole) [46] (C_{dl}=108 μF cm^{-2}) in the initial monomer concentration of 10 mM and for poly(9-benzyl-9*H*-carbazole) [47] (C_{dl}=21.14 μF cm^{-2}) in the initial monomer concentration of 3 mM.

The phase angle is plotted versus the logarithm of the angular frequency. The spectra of the homopolymers and copolymers for various molar fractions had the same appearances towards lower impedances especially at ~10 Hz. The maximum phase angle was obtained as ~73.26° for poly (BzOCz-co-TsP), X_{TsP}=0.83 at the frequency of 15.56 Hz. However, the lowest phase angle (~66.25°) was obtained for poly(BzOCz) at the frequency of 15.56 Hz, as given in Fig. 11.

Based on the $R(Q(RW))$ electrical equivalent circuit, linear Kramers–Kronig (K–K) test was used to simulate the impedance results [48], and then the values of charge transfer resistance (R_{ct}) and R_S were extracted from the fit. The validation of the impedance spectra was done by using (K–K) transformations as described in literature [49, 50]. The double layer capacitance in the circuit of irreversible system was represented by a constant phase element (inset of Fig. 11). Impedance of the constant phase element Z_{CPE} is

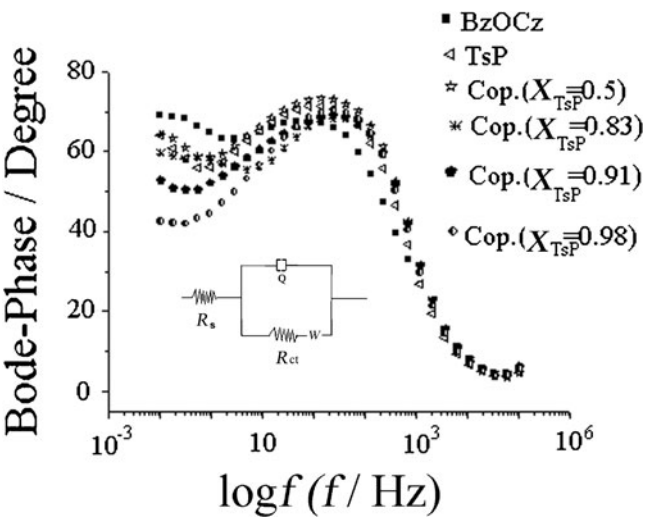

Fig. 11 Bode-phase plot for poly(BzOCz), poly(TsP) and poly (BzOCz-co-TsP) as X_{TsP}=0.5, 0.83, 0.91, and 0.98, respectively. *Inset* Equivalent circuit model of R(Q(RW))

given by $Z_{CPE}=Q_{dl}^{-1}(j\times\omega)^{-n}$, where j is imaginary unit, ω is the angular frequency, Q_{dl} is the double layer pseudo-capacitance of a nonstationary interface [51, 52]. The appearance of the CPE is often related to the electrode roughness or in homogeneity in the conductance or dielectric constant [53]. Q_{dl} turns into the real C_{dl} when the exponent reaches to 1. However, in our system, n varies from 0.72 to 0.78. The deviation of n from unity is a common situation for nonstationary systems due to the frequency independent capacitor [54]. For an ideal capacitor, n is equal to 1. At very low frequencies, the current is almost purely capacitive and the phase angles close to 90°. In literature, ion permeation might occur on poorly self-assembled monolayers, thus increasing the capacitance and decreasing the phase angle at low frequency [55–57]. Warburg impedance (W) is the impedance that results from diffusion of electro-active particles and it is defined by the following equation for the semi-infinite diffusion: $Z_W=A(j\times\omega)^{-0.5}$, where A is Warburg coefficient. W shows higher deviation in our polymer systems.

The two elements of the circuit, R_S and Z_{CPE} that are not affected by the reaction occurring the electrode surface, represent the bulk solution properties and the diffusion of the redox. R_S values CPE and R_{ct} depend on the insulating and barrier properties at the electrolyte/electrode interface [58]. The equation for R_{ct} changing with molar fraction of copolymer at this initial condition was presented by Lasia [59]. $1/R_{ct}$ linearly increases with molar fraction of copolymer. It means that by addition of TsP to the copolymer structure, the copolymer conductivity is higher with higher concentration of TsP monomer in the electrolyte for copolymerization. R_{ct} value of copolymer decreases from 2.48×10^6 Ω for poly(BzOCz) to 9.42×10^5 Ω for $X_{TsP}=0.98$ by increasing the TsP concentration (Table 2). Therefore, total impedance of copolymer is higher than homopolymers. R_{ct} values are obtained as 2.47, 1.97 μΩ for homopolymers of BzOCz and TsP, respectively. And R_{ct} values of copolymer have been obtained as 3.37, 1.72, 1.4, 0.90, and 0.96 μΩ, for $X_{TsP}=0.5$, 0.83, 0.91, 0.98, and 0.99, respectively. Functional groups of copolymer are very important to enhance the capacitance behavior of polymers [60, 61].

Experimental and theoretical values were fitted for combination of Bode magnitude and Bode phase plot in the equivalent circuit model of $R(Q(RW))$, as shown in Fig. 12. The high frequency region of the system (region 3 of Fig. 12) consists of the resistance of the copolymer film R_p and the copolymer capacitance C_p and electrolyte resistance R_E. The medium frequency (region 2 of Fig. 12) can be related to redox process taking place at the copolymer/solution interface given as the R_{ct} and the C_{dl}. The lower frequency (region 3 of Fig. 12) is given by the adsorption of cations and can be described as adsorption resistance parallel to an adsorption capacitance [62].

Conclusıon

In this study, BzOCz and TsP monomers were chemically synthesized to obtain a new copolymer formation. Monomer characterizations were done by FTIR and ^{1}H-NMR spectroscopy. BzOCz and TsP monomers were electrochemically copolymerized on GCE in various molar fractions. Polymer characterizations of poly(BzOCz), poly(TsP), and poly(BzOCz-co-TsP)/GCE were performed via CV, FTIR–ATR, and EIS. The highest electro-active film was obtained for $X_{TsP}=0.98$ compared to poly(BzOCz), poly(TsP), and copolymer of $X_{TsP}=0.5$, 0.83, and 0.91. Double layer capacitance values were obtained as $C_{dl}=\sim14.0$ μF cm^{-2} for poly(BzOCz), poly(TsP), and poly(BzOCz-co-TsP)/GCE. $R(Q(RW))$ electrical equivalent circuit model was used to interpret the impedance data. R_{ct} linearly decreases with molar fraction of copolymer. R_{ct} value of copolymer decreases by incorporation of TsP concentration into the copolymer structure.

Table 2 Equivalent circuit components of $R(Q(RW))$ for poly (BzOCz), poly(TsP) and copolymer at various molar fractions X_{TsP}= 0.5, 0.83, 0.91, and 0.98

Polymers	Equivalent circuit components of $R(Q(RW))$					
	Rs/Ω	$Q/S\times s^{-n}$	n	Rct/Ω	$W/S\times s^{-n}$	x^2
Poly(BzOCz)	158.3	1.07×10^{-5}	0.77	2.48×10^6	7.29×10^{10}	1.47×10^{-3}
Poly(TsP)	129.5	1.00×10^{-5}	0.77	1.98×10^6	4,208	1.96×10^{-3}
Copolymer $X_{TsP}=0.5$	126.5	7.43×10^{-6}	0.78	3.37×10^6	5.6×10^4	1.98×10^{-3}
$X_{TsP}=0.83$	128.9	1.08×10^{-5}	0.72	1.73×10^6	4.13×10^{11}	2.56×10^{-3}
$X_{TsP}=0.91$	127.1	9.96×10^{-6}	0.73	1.41×10^6	2.78×10^8	2.52×10^{-3}
$X_{TsP}=0.98$	124.4	1.09×10^{-5}	0.73	9.42×10^5	3.96×10^4	3.90×10^{-3}

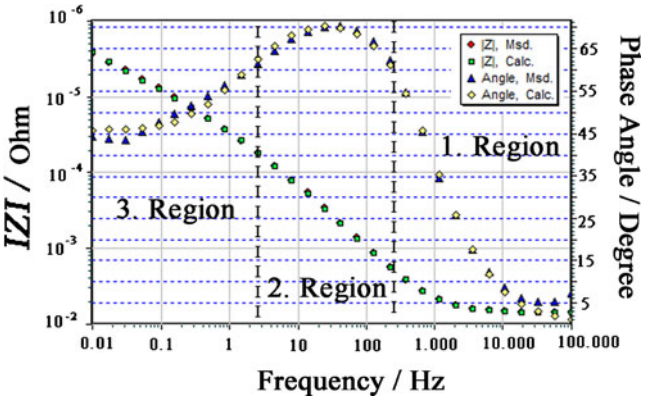

Fig. 12 Bode magnitude–phase graph obtained by simulation ZSimpWin 3.10 program

Acknowledgment The authors thank Prof. Dr. A. Sezai Sarac (Istanbul Technical University, Electropol. Laboratory, Istanbul, Turkey) for providing opportunity to use laboratory facilitates.

References

1. Wan MX (2008) Conducting polymers with micro or nanometer structure. Tsinghua University Press, Beijing
2. He H, Zhu J, Tao NJ, Nagahara LA, Amlani I, Tusi R (2001) J Am Chem Soc 123:7730–7731
3. Bof Bufon CC, Heinzel T (2006) Appl Phys Lett 89:012104–3
4. Lu WK, Elsenbaumer RL, Wessling B (1995) Synth Met 71:2163–2166
5. Pernaut JM, Reynolds JR (2000) J Phys Chem B 104:4080–4090
6. Kasama D, Takata R, Kajii H, Ohmori Y (2009) Thin Solid Films 518:559–562
7. Yeh JM, Chen CL, Chen YC, Ma CY, Lee KR, Wei Y, Li S (2002) Polymer 43:2729–2736
8. Inzelt G, Pineri M, Schultze JW, Vorotynstev MA (2000) Electrochim Acta 45:2403–2421
9. Kim SY, Lee KH, Chin BD, Yu JW (2009) Solar Energy Materials & Solar Cells 93:129–135
10. Zhu R, Li G, Huang G (2009) Mater Corros 60:34–39
11. Giraudeau A, Schaming D, Hao J (2010) J Electroanal Chem 638:70–75
12. Samet Y, Kraiem D, Abdelhedi R (2010) Prog Org Coat 69:335–343
13. Gupta B, Singh AK, Prakash R (2010) Thin Solid Films 519:1016–1019
14. Cloutet E, Yammine P, Ades D, Siove A (1999) Synth Met 102:1302–1303
15. Pandey PC, Prakash RJ (1998) Electrochem Soc 145:4103–4107
16. Morin JF, Boudreault PL, Leclerc M (2002) Macromol Rapid Commun 23:1032–1036
17. Huang J, Niu YH, Yang W, Mo YQ, Yuan M, Cao Y (2002) Macromolecules 35:6080–6082
18. Abe SY, Bernede JC, Delvalle MA, Tregouet Y, Ragot F, Diaz FR, Lefrant S (2002) Synth Met 126:1–6
19. Meng H, Chen ZK, Yu WL, Pei J, Liu XL, Lai YH, Huang W (1999) Synth Met 100:297–301
20. Tran-Van F, Henri T, Chevrot C (2002) Electrochim Acta 47:2927–2936
21. Huang J, Xu YS, Hou Q, Yang W, Yuan M, Cao Y (2002) Macromol Rapid Commun 23:709–712
22. Wang J, Lu B, Liu C, Xu J, Pei M (2010) J Mater Sci 45:5769–5777
23. Liu C, Lu B, Fan C, Xu J, Li Y, Jiang F (2010) J Solid State Electrochem 14:1153–1161
24. Nie G, Xu J, Zhang S, Cai T, Han X (2006) J Appl Polym Sci 102:1877–1885
25. Sriwichai S, Baba A, Deng S, Huang C, Phanichphant S, Advincula RC (2008) Langmuir 24:9017–9023
26. Sarac AS, Ates M, Parlak EA (2005) Int J Polym Mater 54:883–897
27. Sarac AS, Dogru E, Ates M, Parlak EA (2006) Turkish J Chem 30:401–418
28. Bilal S, Holze R (2006) J Electroanal Chem 592:1–13
29. Doherty WJ, Wysocki RJ, Armstrong NR, Saavedra SS (2006) Macromolecules 39:4418–4424
30. Nelson KL (1964) In: Olah GA (ed) Friedel-Crafts and related reactions. Wiley, New York, pp 1024–1032
31. Cerfontain H (1968) Mechanistic aspects in aromatic sulfonation and desulfonation. Wiley, New York
32. Alp C, Ekinci D, Gultekin MS, Senturk M, Sahin E, Kufrevioglu OI (2010) Bioorg Med Chem 18:4468–4474
33. Kitzing R, Fuchs R, Joyeux M, Prizbach H (1968) Helv Chim Acta 51:888–895
34. Binst V, Baert RB, Salsmans R (1973) Synth Commun 3:302–304
35. Nonoyama M (1988) Inorg Chim Acta 145:53–56
36. Papadopoulos EP, Haider NF (1968) Tetrahedron Lett 14:1721–1723
37. Xu J, Nie G, Zhang S, Han X, Hou J, Pu S (2005) J Mater Sci 40:2867–2873
38. Janosik T, Shirani H, Wahlstrom N, Malky I, Stensland B, Bergman J (2006) Tetrahedron 62:1699–1707
39. Saraswathi R, Gerard M, Mahotra BD (1999) J Appl Polym Sci 74:145–150
40. Papez V, Inganas O, Cimrova V, Nespurek S (1991) J Electroanal Chem 282:123–139
41. Ates M, Uludag N, Sarac AS (2011) Mater Chem Phys 127:120–127
42. Inzelt G (2003) J Solid State Electrochem 7:503–510
43. Raoof JB, Ojani R, Beittollahi H, Enzadeh RH (2006) Electroanalysis 18:1193–1201
44. Ates M, Uludag N, Sarac AS (2011) Fibers and Polymers 12:8–14
45. Láng G, Inzelt G (1999) Electrochim Acta 44:2037–2051
46. Ates M, Uludag N (2010) Fibers and Polymers 11:331–337
47. Ates M, Uludag N (2011) Fibers and Polymers 12:296–302
48. Boukamp BA (2004) Solid State Ionics 169:65–73
49. Martinusz K, Láng G, Inzelt G (1997) J Electroanal Chem 433:1–8
50. Láng G, Kocsis L, Inzelt G (1993) Electrochim Acta 38:1047–1049
51. Ragoisha GA, Bondarenko AS (2004) Surf Sci 566–568:315–320
52. Bondarenko AS, Ragoisha GA, Osipovich NP, Streltsov EA (2006) Electrochem Commun 8:921–926
53. Göhr H (1981) Ber Bunsenges Phys Chem 85:274–280
54. Ragoisha GA, Bondarenko AS, Osipovich NP, Streltsov EA (2004) J Electroanal Chem 565:227–234
55. Boubour E, Lennox RB (2000) Langmuir 16:4222–4228
56. Boubour E, Lennox RB (2000) Langmuir 16:7464–7470
57. Boubour E, Lennox RB (2000) J Phys Chem B 104:9004–9010
58. Yang L, Wei W, Xia J, Tao H, Yang P (2005) Anal Sci 21:679–684
59. Lasia A (1999) In: Conway BE, White R (eds) Modern aspects of electrochemistry. Kluwer, New York
60. Liu X, Osaka TJ (1997) Electrochem Soc 144:3066–3071
61. Biniak S, Dziaelendziak B, Siedlewski J (1995) Carbon 33:1255–1263
62. Fikus A, Rammelt U, Plieth W (1999) Electrochim Acta 44:2025–2035